ARTICLES

Photocatalytic growth and plasmonic properties of Ag nanoparticles on TiO$_2$ films

Shuai Li, Qiang Tao, Da-Wei Li, Kun Liu, and Qing-Yu Zhang[a]
Key Laboratory of Materials Modification by Laser, Ion and Electron Beams, School of Physics & Opto-electronic Technology, Dalian University of Technology, Dalian 116024, China

Using nanoparticulate TiO$_2$ films, the photocatalytic growth of Ag nanoparticles (NPs) in the AgNO$_3$ aqueous solution has been studied in terms of reduction, nucleation, and coalescence. It was proved that Ag primary particles were formed in a growth time of <1 s after the photocatalysis started. The growth dynamics was found to be critical for isotropic and anisotropic growth of Ag NPs, depending on the AgNO$_3$ concentration and surface properties of TiO$_2$ films. In the AgNO$_3$ solutions of ≤300 mg/L, the isotropic growth dominates the growth dynamic behavior, producing irregularly spherical Ag NPs. In the AgNO$_3$ solutions of ≥400 mg/L, the increased reduction rate promotes the formation of Ag nanoplates in the product. Ostwald ripening and oriented attachment were suggested to be the mechanisms dominating the isotropic and anisotropic growth, respectively. A photocatalytic growth model of Ag NPs was proposed by taking Ag atom and Ag$^+$ ion diffusion into consideration. The plasmonic properties of the Ag–TiO$_2$ films were studied in terms of extinction, surface enhanced Raman scattering, and fluorescence enhancement.

I. INTRODUCTION

TiO$_2$ is the most promising material in the field of photocatalysis because of its superior photocatalytic activity, chemical stability, low cost, and nontoxicity. As such, its performances in photocatalytic degradation of chemical pollutants and solar energy conversion have been widely studied in the past decades, and its practical application has been seriously considered.[1,2] TiO$_2$ assembled with Ag nanoparticles (NPs) has received much attention because such a hybrid can effectively separate the charges and redshift the absorption to visible light via plasmonic resonance.[3–5] For example, Awazu et al. combined TiO$_2$ and Ag core/SiO$_2$-shell NPs in a heterostructure and the photocatalytic activity was enhanced by a factor of 7 under near-ultraviolet (UV) irradiation.[4] TiO$_2$ assisted by the localized surface plasmon resonance (LSPR) is promising in applications such as photocatalysis,[3–5] photovoltaic cells,[6,7] reversible imaging,[8] LSPR sensors,[9] etc.

Photocatalytic synthesis is a cost-effective way to fabricate Ag–TiO$_2$ films. Using TiO$_2$ films as the photocatalytic reduction media, the Ag$^+$ ions in the AgNO$_3$ solution are reduced on TiO$_2$ films under UV irradiation, forming TiO$_2$-catalyzed Ag NP films, which have been used as the substrates for surface enhanced Raman scattering (SERS).[10,11] However, the growth dynamics of Ag NPs

still remains an open question and has attracted fundamental interest. Ag NPs synthesized by photocatalytic reduction generally exhibit irregular sphere-like shapes. Recently, the photocatalytic growth of anisotropic Ag NPs on the TiO$_2$ films in the AgNO$_3$ ethanol solution was reported, and the vertical growth of Ag nanoplates was attributed to the surface roughness and random features of substrate.[12,13] Using an annealed single-crystalline TiO$_2$ substrate, Kazuma et al. reported the bi- and uniaxially oriented growth of Ag NPs.[14] The preferential orientation and morphology of these Ag NPs were found depending on the presence of ethanol, acetaldehyde, and UV exposure conditions. Though the photocatalytic reduction method has been widely used for fabricating Ag–TiO$_2$ films, studies involving the growth mechanism of Ag NPs are unavailable. In this study, the Ag NP growth in the AgNO$_3$ aqueous solution was systematically studied in terms of reduction, nucleation, and coalescence via morphological characterization and in situ extinction spectroscopy. A photocatalytic growth model was proposed, and the plasmonic properties of the Ag–TiO$_2$ films were studied.

II. EXPERIMENTAL DETAILS

A. Preparation of TiO$_2$ films

The nanoparticulate TiO$_2$ films used for the growth of Ag NPs were prepared using a conventional sol–gel method. First, solutions A and B were prepared by

mixing 3 mL acetylacetone in 50 mL titanium isopropoxide and by adding 0.21 mL nitric acid and 1.4 mL deionized water to 150 mL ethyl alcohol, respectively. After mixing, solutions A and B were stirred for 10 min. All the chemicals used in the preparation were of analytical reagent grade and were purchased from Kermel Chemical Reagents Co. Ltd. Subsequently, the TiO$_2$ sol was prepared by adding solution B dropwise to solution A under vigorous stirring, and then stirred for 2 h at room temperature. The TiO$_2$ sol was aged for 2 days before use. Finally, the TiO$_2$ gel films were coated on the substrate of a cleaned glass slide via a dip-coating method. The TiO$_2$ gel films were heated at 550 °C for 1 h in a muffle furnace to obtain nanoparticulate TiO$_2$ films. The TiO$_2$ films were controlled at a thickness of ~100 nm.

B. Growth of Ag NPs

Ag NPs were grown in the AgNO$_3$ aqueous solution under UV irradiation by a low-pressure mercury lamp (Philips TUV, Amsterdam Noord-Holland, Holland, 8 W). The UV photon (>3.1 eV) flux was estimated to be 10^{16}/cm^2·s when fixing the lamp at a distance of TiO$_2$ film of ~6 cm. The experimental setup is depicted in Fig. 1, and the Ag NP growth was performed in a dark room and monitored by in situ extinction spectrum measurement using a UV–visible–near-infrared spectrometer (UV–Vis–NIR, Ocean Optics, Maya 2000-Pro, Dunedin FL). 50–3200 mg/L (~0.3 to ~18.8 mM) AgNO$_3$ aqueous solutions were used for the study on the growth dynamics of Ag NPs. After the growth was stopped, the samples were immediately taken out and were carefully cleaned, and then dried with a slow flow of dry nitrogen.
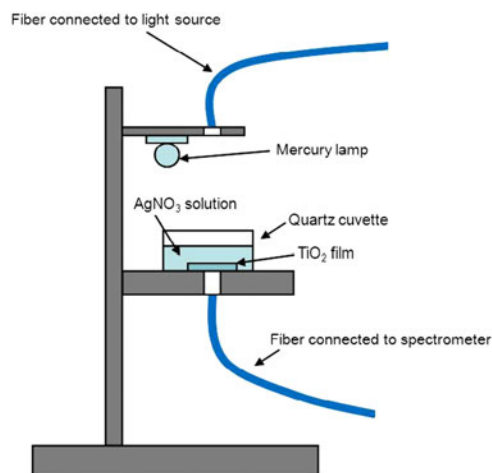
C. Characterization of Ag–TiO$_2$ films

Scanning electron microscopy (SEM, Hitachi, S-4800, Tokyo, Japan) was used to characterize the morphology of Ag–TiO$_2$ films. The SEM images were statistically analyzed to obtain the size distribution of Ag NPs. Transmission electron microscopy (TEM, Hitachi, H800, Tokyo, Japan) was used to study the crystal structure of Ag nanoplates. The roughness of Ag–TiO$_2$ films was determined by atomic force microscopy (AFM, Benyuan, CSPM 5000, Shenzhen, China). Using 10 μM Rhodamine 6G (R6G) ethanol solution as the probe, the SERS activity of the Ag–TiO$_2$ films was evaluated by collecting Raman signals under excitation of a He–Ne laser operating at ~3.5 mW with a Raman spectroscope (Renishaw inVia plus, Renishaw, Wotton-under-Edge Gloucestershire, UK). Raman enhancement factor (EF$_{SERS}$) was calculated using the Raman spectrum of 0.1 M R6G solution on a pure TiO$_2$ film as the reference and by taking the numbers of R6G molecules within the irradiated area into account. Rhodamine B (RhB) was used as the fluorophore to study the fluorescence enhancement. To avoid fluorescence quenching due to a direct contact of fluorophore with Ag NPs, 1 mM RhB was added to TiO$_2$ sol–gel, and then coated on Ag–TiO$_2$ films by a spin-coating method. Photoluminescence (PL) and PL excitation (PLE) spectra were measured using a FLS 920 fluorescence spectrometer (Edinburgh Instruments Ltd., Scotland, U.K.) under excitation of a Xe lamp. Time-resolved spectroscopy was used to study the PL decay under excitation of a 405 nm laser diode with a pulse width of <80 ps and a repetition frequency of 20 MHz. The average PL lifetimes of RhB molecules were obtained by fitting the time-resolved PL spectra with a double exponential function.

III. RESULTS AND DISCUSSION

A. Isotropic growth of Ag NPs

Figure 2 shows the typical morphology of isotropic Ag NPs, which were grown in the 180 mg/L (~1 mM) AgNO$_3$ solution. The SEM images show that the Ag NPs at the growth time of 2, 4, 8, 16, and 120 min exhibited irregularly spherical shapes. At a 2 min growth time, the Ag NPs are ~27 nm of average size and ~4 × 10^9/cm^2 of density. When increasing the growth time to 4 min, the Ag NP density dramatically reduced to ~2.3 × 10^6/cm^2, and the size increased to ~97 nm, indicating that the coalescence process took place between Ag primary particles at a growth time in between 2–4 min. By fitting the time dependence of average size (d) after the coalescence phenomenon, we found $d^3 \propto t$, as shown in Fig. 2(f). Such a relationship is an indication of diffusion-limited growth. In other words,

FIG. 1. Schematic experimental setup and the in situ monitoring system of extinction spectroscopy.
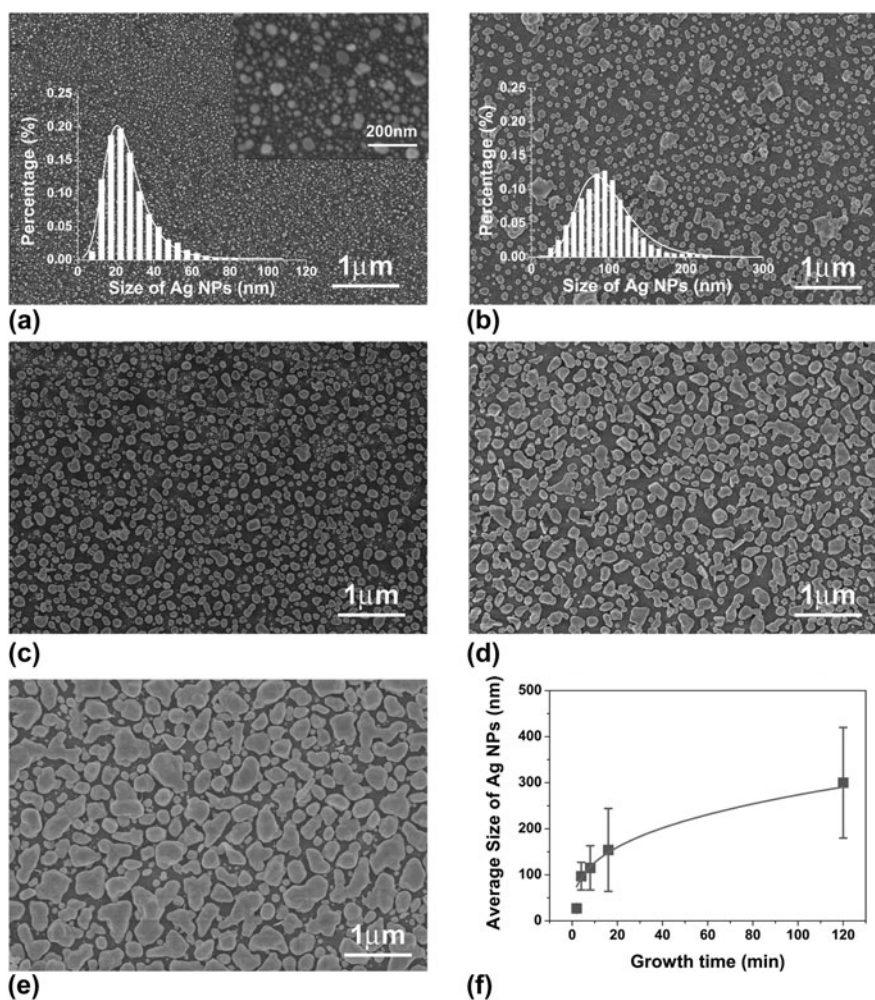
FIG. 2. (a–e) SEM images of Ag–TiO$_2$ films grown in 180 mg/L AgNO$_3$ solution at the growth time of 2, 4, 8, 16, and 120 min, respectively. The insets in (a) and (b) are the size distributions of Ag NPs. (f) Growth-time dependence of Ag NP size.

Ostwald ripening (OR)[15] dominates the coarsening process of Ag NPs.

Ex situ SEM observation is incapable of detecting the dynamic process of Ag NP growth and cannot provide the required resolution to recognize the Ag primary NPs in the nucleation stage. Therefore, in situ extinction spectroscopy was used to study the photocatalytic nucleation of Ag NPs. Figure 3(a) shows the in situ extinction spectra from the photocatalytic beginning to 80 s. The extinction was defined by ln(I_0/I), where I_0 is the transmitted intensity before photocatalytic reduction and I is the intensity during photocatalytic reduction. The extinction spectra were recorded in 13 ms with intervals of 10 s. As shown in the figure, two extinction peaks, which are associated with Ag primary particle density and size, appeared at ~400 and ~510 nm. By plotting the extinction intensity at ~400 nm as a function of growth time, as shown in Fig. 3(b), the formation of Ag primary particles was extrapolated to a time as early as <1 s after the photocatalytic beginning. As a matter of

fact, the extinction of Ag primary particles was observed in the 0-s spectrum, as shown in the inset of the figure, indicating that the nucleation took place truly in a very short time after the photocatalytic reduction started. The extinction spectra show that the number of Ag NPs is increasing with the irradiation time, whereas the change in sizes is not obvious. The formation of Ag primary particles originates from supersaturated Ag atoms, which are related to the photocatalytic reduction ability of TiO$_2$ films. Based on the statistical analysis of Ag NPs, the Ag reduction rate was estimated to be ~2 × 10^{13} cm^{-2} s^{-1}, which is reasonable in comparison with the irradiation photons of ~10^{16} cm^{-2} s^{-1}.

B. Anisotropic growth of Ag NPs

The Ag reduction rate is determined by the parameters related to UV irradiation, reduction activity of TiO$_2$ film, AgNO$_3$ concentration of solution, etc. By increasing the AgNO$_3$ concentration, we found that the
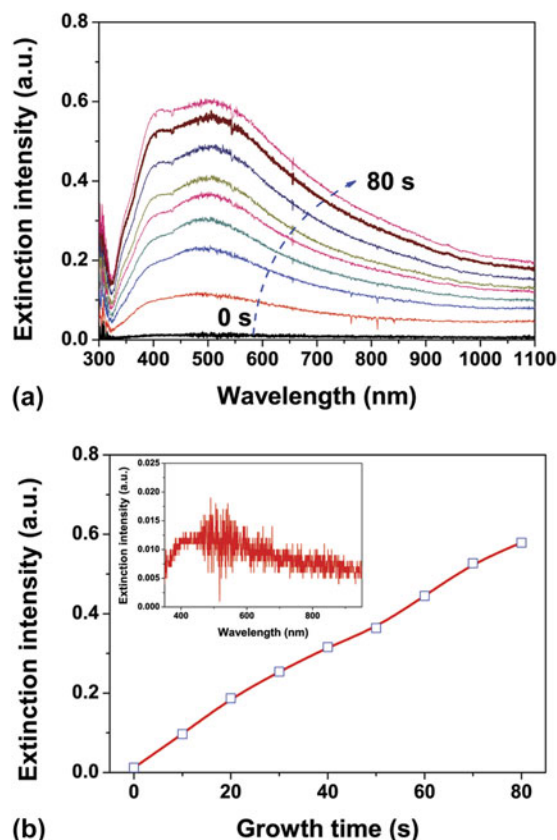
FIG. 3. (a) In situ extinction spectra of Ag NPs grown in 180 mg/L $AgNO_3$ solution from the photocatalytic beginning to 80 s, in which the spectra were recorded in 13 ms with intervals of 10 s. (b) Growth-time dependence of extinction intensity at ~380 nm and the inset is 0-s extinction spectrum.

increased Ag reduction rate gave rise to a change in Ag NP growth, resulting in the formation of Ag nanoplates in the product. Figure 4 shows an example of Ag NP growth in the 2800 mg/L $AgNO_3$ solution. As shown in the figure, a large amount of thin Ag nanoplates were produced at the growth time as early as 2 min. The Ag nanoplates were ~10 nm thick and 0.1–1 μm of edge length. With an increase in the growth time, the sizes of Ag nanoplates were not varied obviously, but the thickness increased. TEM analysis shows that the nanoplates are faced with Ag (111) planes, as shown in Fig. 4(f). At a 120 min growth time, the Ag nanoplates were rarely observed, instead evolved into three-dimensional Ag NPs with the well-defined shapes, which are a little different from the irregular Ag NPs grown in the 180 mg/L $AgNO_3$ solution. The SEM images reveal that the increased $AgNO_3$ concentration promoted an early coalescence resulting in the formation of Ag nanoplates. In other words, the Ag nanoplates were formed in the early period of coalescence, rather than gradually grew up with the increase in the growth time.

Figure 5 shows the in situ extinction spectra from the beginning to 80 s. It is different from the growth of

Ag NPs in the 180 mg/L $AgNO_3$ solution that the extinction in the visible region is slowly increased and the extinction peaks associated with individual Ag NPs are not clearly distinguishable. On the other hand, the extinction in the NIR region is rapidly increased with the increase in the growth time. According to the effective medium theory,[16,17] the enhanced extinction in the NIR region can be attributed to the extreme high-density primary particles and/or the formation of Ag nanoplates. In fact, the Ag nanoplates were formed at a quite early time, because a small extinction peak at ~340 nm, which has been assigned to out-of-plane quadrupole resonance of Ag nanoplates in the $AgNO_3$ solution,[18] emerged in the 30-s spectrum and gradually changed to be clear with the increase in the growth time, as indicated by the arrow in the figure. SEM images show that Ag nanoplates and irregularly spherical Ag NPs were co-existed in the photocatalytic growth using 2800 mg/L $AgNO_3$ solution, whereas the isotropic growth of Ag NPs was restrained. The Ag reduction rate in 2800 mg/L $AgNO_3$ solution was estimated to be ~2×10^{14} cm^{-2} s^{-1}, which is ~10 times of that in 180 mg/L $AgNO_3$ solution. Therefore, we conclude that the increased reduction rate promotes the formation of Ag nanoplates. Such nanoplates are of interest in the fields such as stereoscopic visions, storing multiple information, certification, and anticounterfeit technologies and polarizers,[19,20] because they have three major LSPR modes, namely, out-of-plane mode, in-plane longitudinal and transverse modes, and respond selectively to light polarized in a specific angle.

C. Growth mechanism of Ag NPs

Using 50–3200 mg/L $AgNO_3$ solution, we systematically investigated the photocatalytic growth dynamics of Ag NPs using in situ extinction spectra. As shown in Fig. 6, the extinction spectra reveal that the Ag NPs are of typical isotropic growth in the solutions of ≤300 mg/L and transit into anisotropic growth in the solutions of ≥400 mg/L, indicating that a critical $AgNO_3$ concentration in between 300 and 400 mg/L is needed for the formation of Ag nanoplates. Besides $AgNO_3$ concentration, the surface properties of TiO_2 films were also found to be responsible for the formation of Ag nanoplates. All the films used for the above study were kept in moisture environment for weeks. Using a fresh film, which was immediately used for Ag NP growth after calcination, or using films kept in a dry atmosphere, Ag nanoplates were never obtained by photocatalytic growth in 50–3200 mg/L $AgNO_3$ solutions, suggesting that H_2O absorption modified the surface properties of TiO_2 films and changed the photocatalyic reaction. We believe that the re-oxidation of reduced Ag atoms and the electron–hole recombination are the likely reasons for
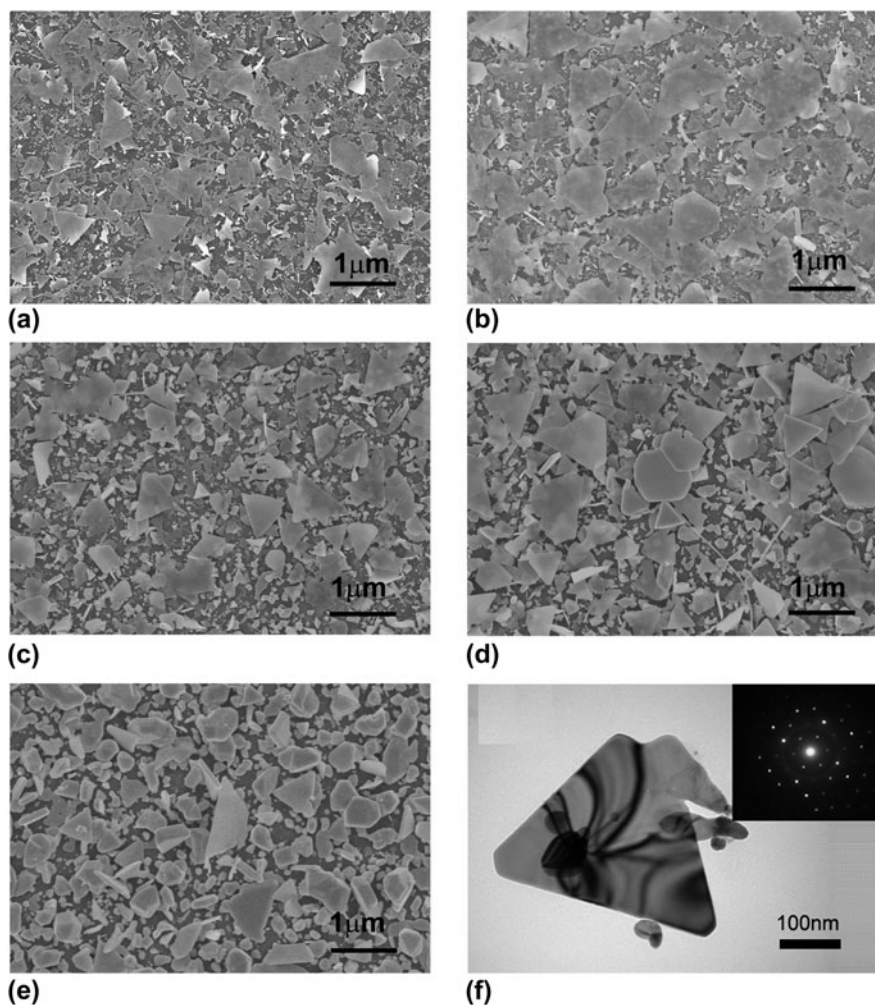
FIG. 4. (a–e) SEM images of Ag–TiO$_2$ films grown in 2800 mg/L AgNO$_3$ solution at the growth time of 2, 4, 8, 16, and 120 min, respectively. (f) TEM image of a triangular Ag nanoplate and diffraction pattern (inset).
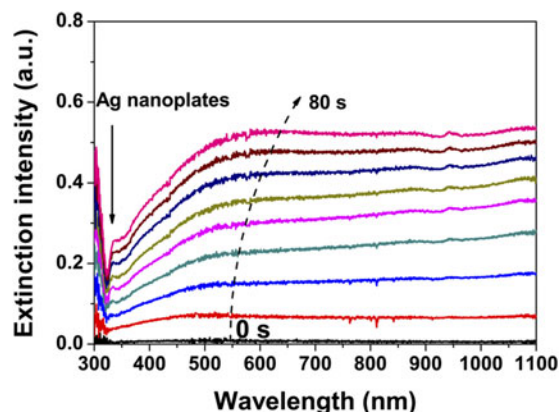

FIG. 5. In situ extinction spectra of Ag nanoplates grown in 2800 mg/L AgNO$_3$ solution from the photocatalytic beginning to 80 s, in which the spectra were recorded in 13 ms with intervals of 10 s.

decrease in Ag reduction rate. To prevent Ag atoms from re-oxidation and/or to effectively separate charges, a layer of vacuum pump oil was coated on the surface of

TiO$_2$ film, and then the anisotropic Ag NP growth was successfully induced,[21] evidencing our assumption.

By carefully observing the SEM images [Figs. 4(a)–4(c)], we found that the nanoplates generally lie on the irregularly spherical NPs, and the small NPs beneath thin nanoplates are visible, indicating that the nanoplates were produced in the solution, rather than on the surface of TiO$_2$ film. In other words, Ag nanoplates were produced primarily in the area adjacent to the film surface, and adhered to the surface when they were taken out from the solution. As a matter of fact, a large amount of low-dimensional Ag nanostructures, such as nanowires, nanoribbons, and nanoplates, had been taken from the solution when the photocatalytic growth of Ag NPs was conducted for a longer time using TiO$_2$ or ZnAlO films as the reduction media, as shown in the supporting material (Fig. S1). To understand the formation mechanism of Ag NPs and Ag nanoplates, we proposed a growth model by taking Ag atom and Ag$^+$ ion diffusion into consideration. Because the solution density is close to that of a solid,
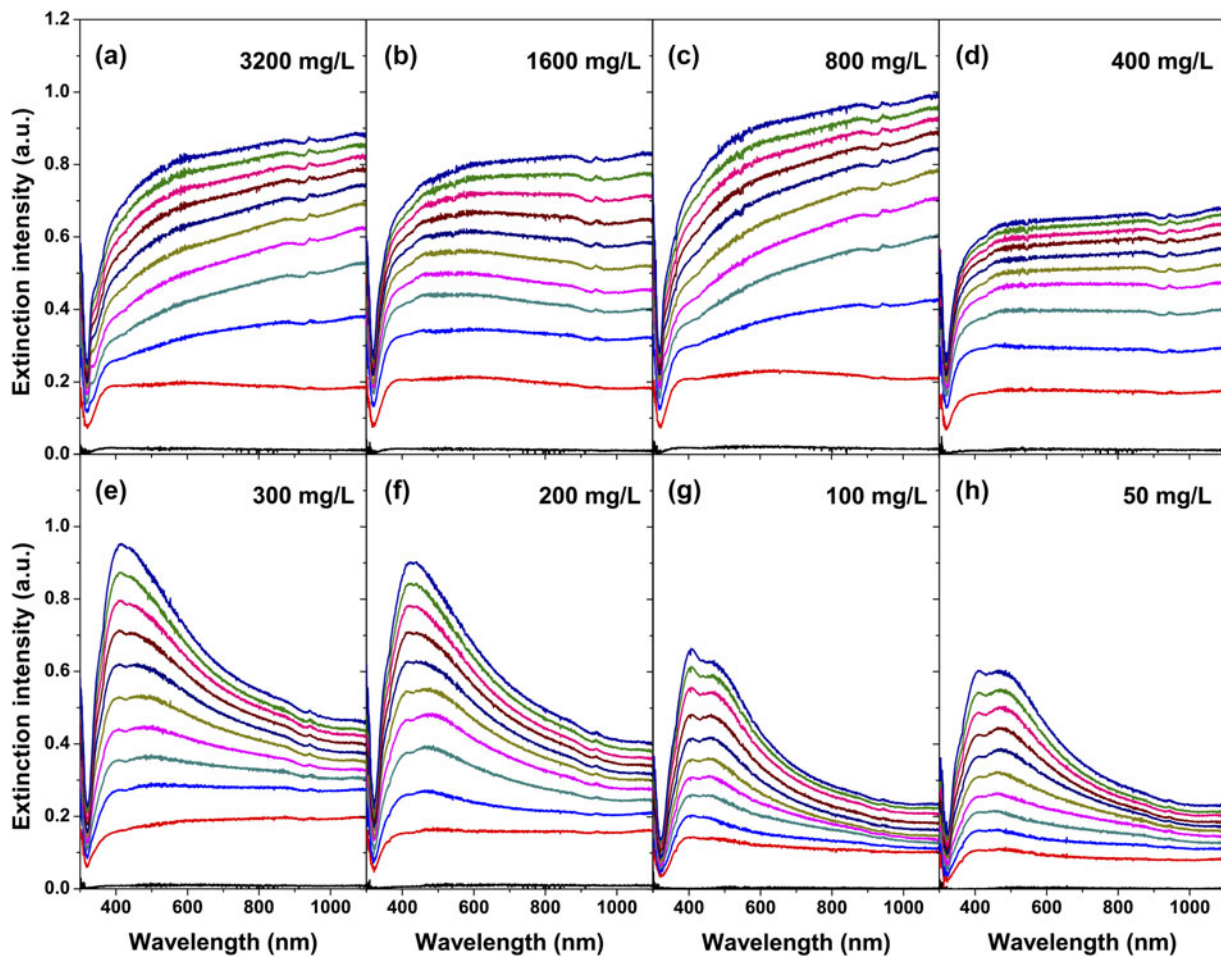
FIG. 6. In situ extinction spectra of Ag–TiO$_2$ films grown in 50–3200 mg/L AgNO$_3$ solutions, in which the extinction spectra were recorded in 13 ms with intervals of 6 min.

the force applied to Ag atoms by the substrate atoms is approximately equal to that by the atoms in the solution. Thus, it is different from the film growth in a vacuum that Ag atoms on the surface of TiO$_2$ film have a large possibility to diffuse into a solution. Considering that the Ag atoms were produced on the surface of TiO$_2$ film by the reduction of Ag$^+$ ions, the one-dimensional diffusion equations and the boundary conditions for Ag atom and Ag$^+$ ion diffusion can be written as

$$\frac{\partial u(x,t)}{\partial t} = D_0 \frac{\partial^2 u(x,t)}{\partial x^2} \quad , \tag{1}$$

$$\frac{\partial v(x,t)}{\partial t} = D_+ \frac{\partial^2 v(x,t)}{\partial x^2} \quad , \tag{2}$$

$$\left.\frac{\partial u(x,t)}{\partial t}\right|_{x=0} = k_R v(0,t) - k_O u(0,t) \quad , \tag{3}$$

$$\left.\frac{\partial v(x,t)}{\partial t}\right|_{x=0} = -k_R v(0,t) + k_O u(0,t) \quad , \tag{4}$$

where $u(x, t)$ and $v(x, t)$ are the Ag and Ag$^+$ densities at position x and at time t, respectively; D_0 and D_+ are the corresponding diffusion coefficients; k_R and k_O are the reduction and oxidation rates. Numerical calculations showed that the reduction on TiO$_2$ film reaches equilibrium with the oxidation in a time scale of $<<1$ ms. Thus, $u(x, t)$ is something like the diffusion function with $u(0, t) = $ constant. Taking the film roughness and the transverse diffusion into account, a specific $u(x, t)$ in Fig. 7(a) is suggested. Once $u(x, t)$ is supersaturated, nucleation is possible. The critical free energy (ΔG_c), critical radius (r_c), and critical density (n_c) of primary particles are related to supersaturated concentration (C) by[22]

$$\Delta G_c = \frac{16\pi\sigma^3}{3} \left[\frac{v_a}{kT \ln(C/C_0)}\right]^2 \quad , \tag{5}$$
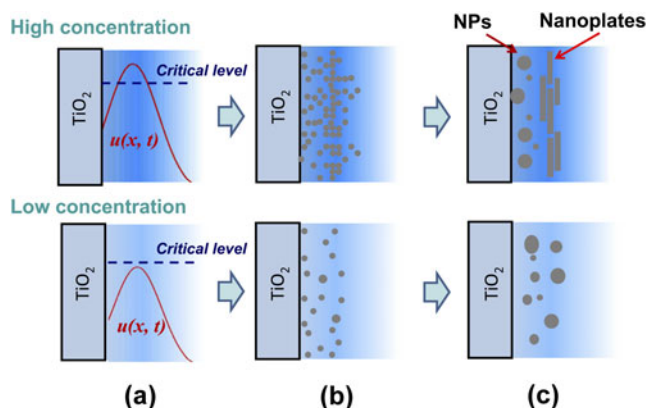
FIG. 7. Photocatalytic growth model of Ag NPs in AgNO$_3$ solution: (a) reduction of Ag atoms, (b) nucleation of Ag primary particles, and (c) coalescence of Ag NPs and/or Ag nanoplates. The top panel is for high AgNO$_3$ concentration and the bottom panel is for low AgNO$_3$ concentration.

$$r_c = \frac{2\sigma v_a}{kT \ln(C/C_0)} \quad , \qquad (6)$$

$$n_c = n_s \exp\left(-\frac{\Delta G_c}{kT}\right) \quad , \qquad (7)$$

where C_0 is the saturated concentration of Ag atoms, σ is the surface free energy density of primary particles, v_a is the atomic volume, and n_s is the number of nucleation sites. Equations (5) and (7) tell us that the distribution $u(x, t)$ of Ag atoms produces nonuniformly distributed primary particles, which might be decisive for the formation of Ag nanoplates or not. According to Eqs. (6) and (7), the large value of $u(x, t)$ produces the high-density and small-size primary particles. Therefore, if the supersaturated $u(x, t)$ is lower than a critical level in the nucleation gestation, the density of primary particles is low, and then the OR mechanism dominates the coalescence process leading to the isotropic growth of Ag NPs. If $u(x, t)$ within a large enough area is higher than the critical level, the density of primary particles is so high that a new coalescence mechanism, probably the oriented attachment (OA) mechanism, promotes the formation of Ag nanoplates, as shown in Figs. 7(b) and 7(c). At the same time, the OR growth still dominates the area where $u(x, t)$ is lower than the critical level, and then the isotropic Ag NPs are present. The restrained isotropic growth of Ag NPs can be attributed to the larger surface free energy of irregular Ag NPs in comparison with that of Ag nanoplates because the atom transfer is always from where surface free energy is high to where surface free energy is low.

The growth model can explain the phenomenon of Ag nanoplates lying on the small Ag NPs. On the other hand, the growth model is consistent with the conclusion of Yin et al. that the OA growth is facilitated in high-density primary particles.[23] Similarly, the formation of Ag nanoplates using AgNO$_3$ ethanol solution[12] or using oil-decorated TiO$_2$ films[21] can also be attributed to the increase in the Ag reduction rate due to the photodegradation of organic molecules. It should be emphasized that the growth model suggested the importance of surface roughness in the formation of Ag nanoplates, which is consistent with the observation of Tanabe et al. that the growth of Ag nanoplates was related to the surface roughness and random features of substrate.[12] According to our growth model, a smooth TiO$_2$ film facilitates the formation of large-scale Ag nanoplates. As a matter of fact, a Ag nanoplate larger than $\sim$10 μm $\times$ 10 μm was obtained by using a smooth TiO$_2$ film, as shown in the supporting material (Fig. S2). On the other hand, the growth model is proposed on the basis of our experimental setup with strong UV irradiation. Under strong UV irradiation, the nucleation on TiO$_2$ films is not important in the photocatalytic growth of Ag NPs because the reduction–oxidation environment does not facilitate the formation of stable Ag primary particles. To realize the epitaxial growth of Ag NPs, we recommend using a low UV photon flux and a single-crystal TiO$_2$ substrate.

D. Extinction spectra of Ag–TiO$_2$ films

Figure 8 shows the extinction spectra of Ag–TiO$_2$ films grown at the growth time of 2, 4, 8, 16, and 120 min. For the films grown in the 180 mg/L AgNO$_3$ solution, the Ag–TiO$_2$ film at 2 min growth time exhibits a UV extinction peak at $\sim$380 nm and a blue–green extinction peak at $\sim$450 nm, as shown in Fig. 8(a). With an increase in the growth time, the UV peak was blue-shifted and the blue–green peak was red-shifted. The two extinction peaks are very like the quadrupole and dipole resonances of Ag spheroids,[24] however, they are more likely due to a combination of factors because visible quadrupoles require extreme size, shape, and external medium regularity in a typical macro geometry which averages over thousands of particles. In other words, the extinction spectra are the hybridized plasmon response of the complex nanostructures[25] or due to an asymmetric dielectric environment.[26] When increasing the growth time, the extinction peak at $\sim$380 nm was rapidly enhanced and the extinction peak at $\sim$450 nm was weakened. The extinction peak at $\sim$450 nm was no more observed for the Ag–TiO$_2$ film at a 120 min growth time.

For the Ag–TiO$_2$ film grown in the 2800 mg/L AgNO$_3$ solution at 2 min growth time, the extinction spectrum is something like that of a smooth and compact Ag film, and no particle-like extinction peak was observed, as shown in Fig. 8(b), indicating that the Ag nanoplates with various sizes dominate the extinction of the Ag–TiO$_2$ film. With the increase in the growth time,
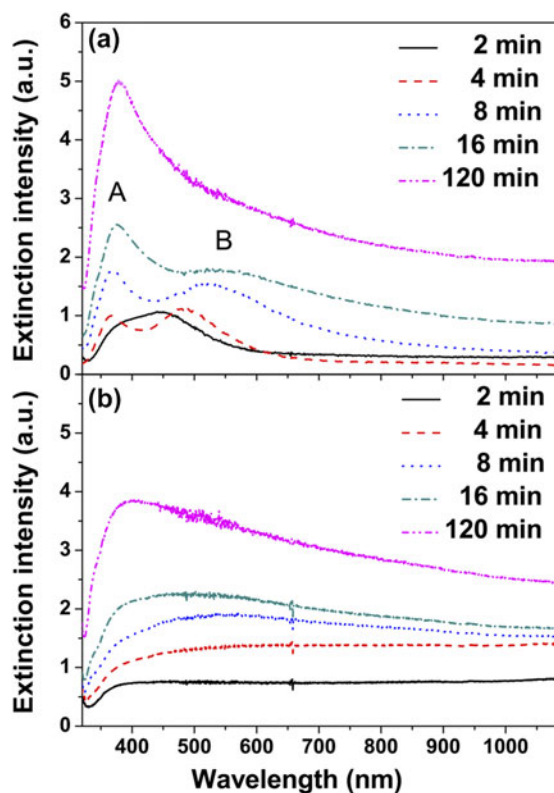
FIG. 8. Extinction spectra of Ag–TiO₂ films at the given growth times: (a) Ag–TiO₂ films grown in 180 mg/L AgNO₃ solution and (b) Ag–TiO₂ films grown in 2800 mg/L AgNO₃ solution.

the particle-like extinction emerges and gradually changes to be visible. By observing the SEM images presented in Fig. 4, we suggest that the particle-like extinction results from the transition of Ag nanoplates to the Ag NPs with well-defined shapes. At 120 min growth time, the extinction spectrum changed to be similar to that of the Ag–TiO₂ film grown in 180 mg/L AgNO₃ solution, which is in accordance with SEM observation.

E. SERS of Ag–TiO₂ films

Using R6G as the probe molecule, the SERS activity of the Ag–TiO₂ films was evaluated. Figure 9(a) shows the Raman spectra of R6G molecules on Ag–TiO₂ films grown in 180 mg/L AgNO₃ solution at the growth time of 2, 4, 8, 16, and 120 min. The R6G featured bands are identified to be the in-plane bending vibration of C–C–C ring at 612 cm⁻¹, the out-of-plane and in-plane bending vibrations of C–H at 770 and 1130 cm⁻¹, and aromatic stretching vibrations at 1362, 1510, and 1650 cm⁻¹.[27,28] The Raman intensities increased when increasing the growth time from 2 to 120 min. Using the Raman intensity of 0.1 M R6G on a pure TiO₂ film as the reference, EF_{SERS} was determined by carefully calculating the number of R6G molecules within the irradiation area. The Ag–TiO₂ film at 120 min growth time exhibits an enhancement
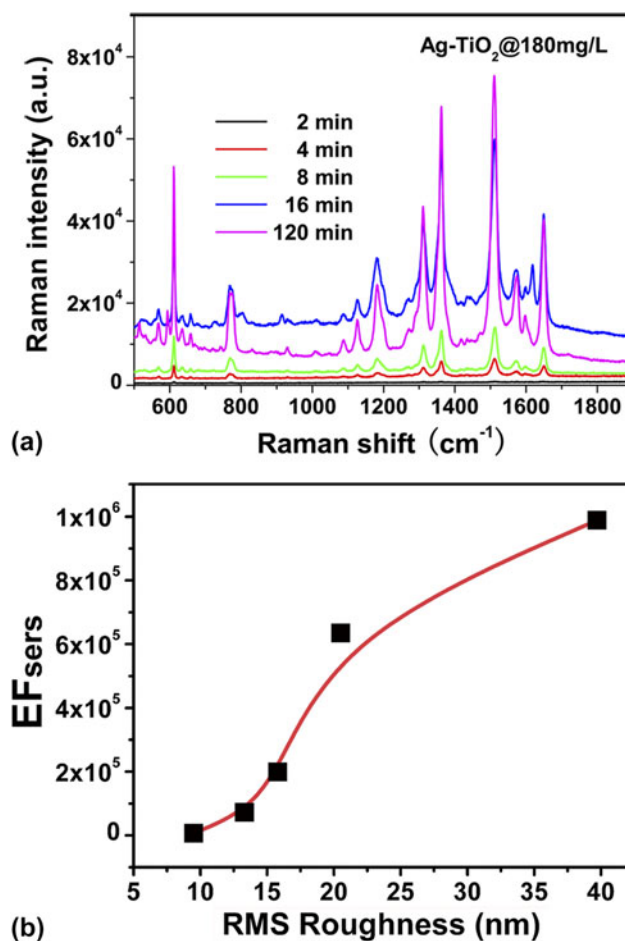

FIG. 9. (a) Raman spectra of R6G molecules on Ag–TiO₂ films that were grown in 180 mg/L AgNO₃ solution at the given growth time. (b) SERS enhancement factor as a function of the film surface roughness.

factor of ∼10⁶, indicating that such a cost-effective Ag–TiO₂ film is available for SERS applications.

Two kinds of electromagnetic "hot spots", the sub-10 nm "feed-gaps" between metal NPs and the "lightning rods",[29,30] have been known making the important contributions to SERS. Based on our SEM observation, the "feed-gaps" were excluded because the adjacent Ag NPs are generally separated by a distance larger than 10 nm. Thus, "lightning rods" are proposed to be the SERS mechanism of Ag–TiO₂ films. To demonstrate our proposal, AFM was used to quantitatively measure the roughness of Ag–TiO₂ films, and the roughness dependence of EF_{SERS} is plotted in Fig. 9(b). EF_{SERS} increased with the roughness of Ag–TiO₂ films, indicating that the enhanced Raman signals can be attributed to the "lightning rods" effect at the sharp edges of Ag NPs, similar to the SERS mechanism on a rough Ag metal surface.

Similar to the films grown in 180 mg/L AgNO₃ solution, the Ag–TiO₂ films grown in 2800 mg/L AgNO₃

solution extremely enhanced the Raman signals of R6G molecules, as shown in Fig. 10(a). Figure 10(b) shows the growth-time dependence of SERS enhancement factor, and the EF_{SERS} values of the Ag–TiO$_2$ films grown in 180 mg/L AgNO$_3$ solution are also plotted for comparison. The Ag–TiO$_2$ films dominated by Ag nanoplates, which are the two samples grown in 2800 mg/L AgNO$_3$ solution for 2 and 4 min, produced a $\sim 1 \times 10^5$ Raman enhancement, which is larger than that of Ag–TiO$_2$ films with small Ag NPs, but smaller than that of Ag–TiO$_2$ films with large Ag NPs. With the increase in the growth time, the EF_{SERS} values increased. The increase of EF_{SERS} values can be ascribed to the transition of Ag nanoplates to Ag NPs with well-defined shapes, increasing the density of large Ag NPs. However, the production of large Ag NPs in 2800 mg/L AgNO$_3$ solution is lower than that in 180 mg/L AgNO$_3$ solution, as shown in Fig. 4(e). Therefore, the increase in Raman enhancement is limited when the growth time was extended to 120 min. The results

suggest that using a high concentration solution cannot bring large SERS values due to the formation of Ag nanoplates.

F. Enhanced fluorescence of Ag–TiO$_2$ films

Silver island films were studied in fluorescence enhancement, but few reports involved the Ag–TiO$_2$ film with high-density Ag NPs. Using RhB as the fluorophore, we studied the fluorescence enhancement of the Ag–TiO$_2$ films grown in 180 mg/L AgNO$_3$ solution. The fluorophore of 1 mM RhB in TiO$_2$ sol–gel was coated on the surface of Ag–TiO$_2$ films to avoid the fluorescence quenching. The average distance between the fluorophores is $\sim$12 nm, larger than Forster distance (4.2 nm) for the homoresonance energy transfer, and the fluorophore density was estimated to be $\sim 6 \times 10^{15}$ cm^{-2} in a 100 nm layer adjacent to the surface of Ag NPs. Considering that the PL spectrum strongly depends on excitation photon energy, we first measured the absorption, PL, and PLE spectra of RhB in solution to determine the excitation wave length. As shown in Fig. 11(a), the PLE spectrum was found essentially superposed with the absorption, and the maximum PLE at 554 nm partially overlapped with PL emission, thus the excitation light for PL measurement was set at the wave length of 500 nm. Similar RhB PL spectra on the pure TiO$_2$ films were obtained and the PL intensity did not obviously depend on the thickness of fluorophore layer, as shown in the inset of Fig. 11(a), in which the RhB PL spectra of the samples with different thick fluorophore layers are presented. Compared to the RhB fluorescence on the pure TiO$_2$ films, the PL intensity of RhB on the Ag–TiO$_2$ films was enhanced and the enhancement strongly depends on the growth time of Ag NPs, as shown in Fig. 11(b). Using the RhB PL spectra on the pure TiO$_2$ as the reference, the enhancement factor (EF_{PL}) was determined to be 1.5–6.9, as shown in the inset of Fig. 11(b). The enhancement is consistent with the measurement for the other fluorophore on the silver island films.[31]

Fluorescence enhancement results primarily from two processes, an increase of the localized electromagnetic fields near the metal NPs and an increase of radiative decay rate.[32] Thus, $EF_{PL} = G_{exc} \times G_{QY}$, where G_{exc} is the enhancement of the localized electromagnetic field, and G_{QY} is the increase in quantum yield of the fluorophore, which can be estimated with the PL lifetime. For the RhB molecules on the pure TiO$_2$ films, the determined average lifetime was 0.63 ± 0.14 ns. The RhB PL lifetime on the Ag–TiO$_2$ films was found to be 0.35–0.58 ns and did not obviously depend on the growth time of Ag NPs. Considering that the quantum yield of a fluorophore in solid cannot exceed a few percents, G_{QY} was estimated smaller than 2. Thus, the localized electromagnetic field
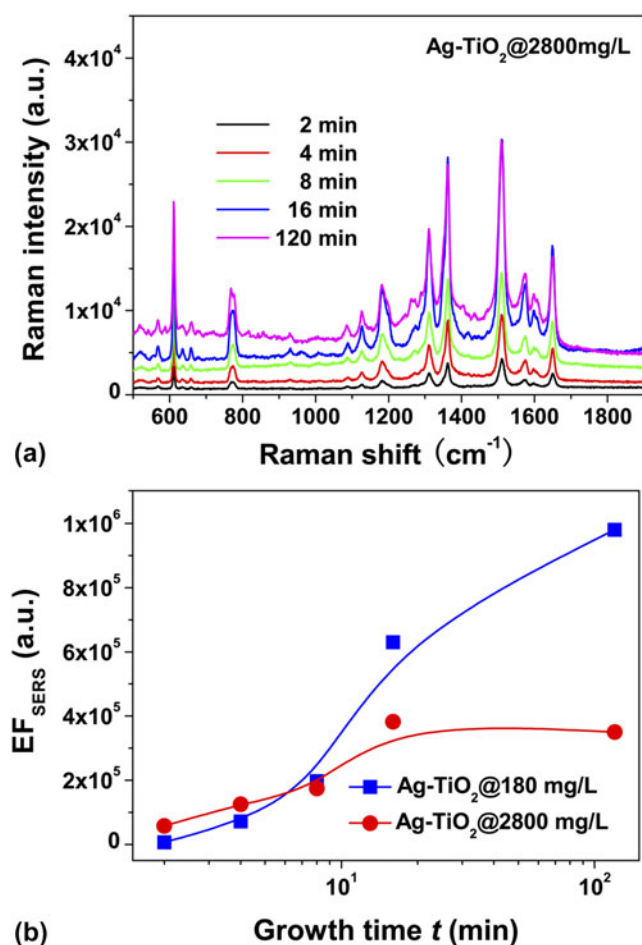

FIG. 10. (a) Raman spectra of R6G molecules on Ag–TiO$_2$ films that were grown in 2800 mg/L AgNO$_3$ solution at the given growth time. (b) SERS enhancement factor as a function of the growth time.
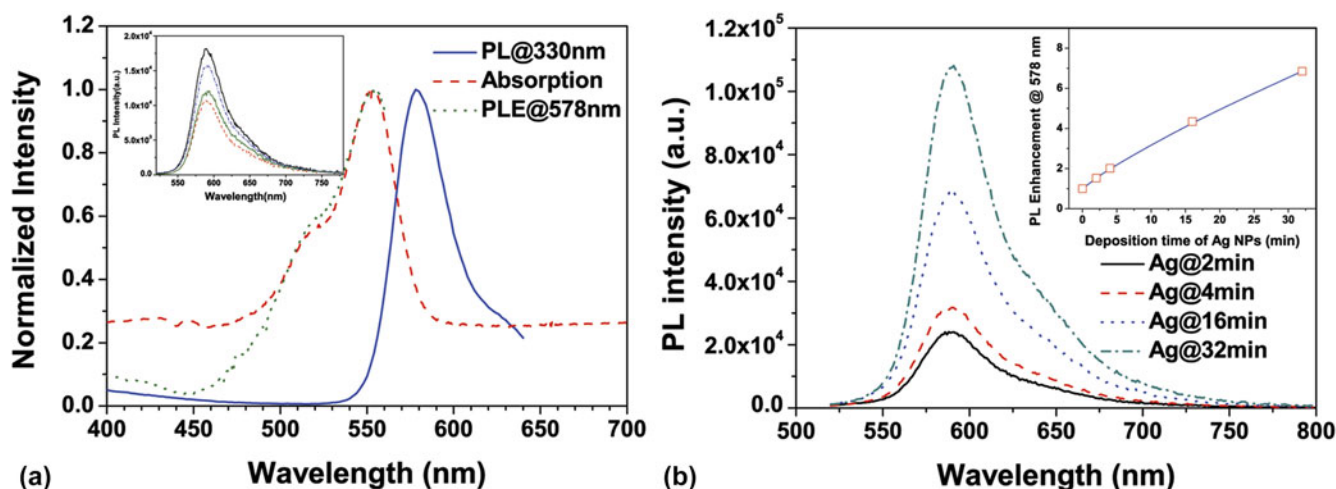
FIG. 11. (a) Absorption, PL, and PLE spectra of RhB solution. The PL spectrum was excited by 330 nm light and the PLE spectrum was detected at 578 nm. The inset shows RhB PL spectra on pure TiO₂ films. (b) RhB PL spectra on Ag–TiO₂ films that were grown in 180 mg/L AgNO₃ solution at the given growth time.

and/or the increased scattering of the Ag–TiO₂ films play an important role in the PL enhancement of RhB besides the increase in quantum yield. In addition, the increased roughness of the Ag–TiO₂ film by deposition time might result in larger surface area allowing more dye molecules located in the near field of the Ag nanostructures, thus leading to more enhancement of PL intensity.

IV. CONCLUSIONS

Growth dynamics of Ag NPs by photocatalytic reduction is critical for isotropic and anisotropic growth of Ag NPs, depending on the AgNO₃ solution concentration and the reduction ability of TiO₂ films. For the photocatalytic growth of Ag NPs on the TiO₂ films under the given UV irradiation in this study, a critical AgNO₃ concentration in between 300 and 400 mg/L is determined for the transition from isotropic growth to anisotropic growth. In the solutions lower than the critical concentration, the isotropic growth is the predominant mechanism that leads to the formation of irregularly spherical Ag NPs. In the solutions higher than the critical concentration, the increased reduction rate promotes the formation of Ag nanoplates in the product. Nucleation of Ag primary particles was demonstrated taking place as soon as in a time scale of <1 s after the beginning of photocatalysis. By taking the diffusion of Ag atoms into consideration, a photocatalytic growth model was proposed and the primary particle density was suggested, which plays a decisive role in the formation of Ag nanoplates. OR dominates the isotropic growth of Ag NPs for the low-density primary particles and OA growth is the mechanism responsible for the formation of Ag nanoplates when the density of primary particles is high. The plasmonic properties of Ag–TiO₂ films with

Ag nanoplates are a little different from those of Ag–TiO₂ films with irregularly spherical Ag NPs. For the Ag–TiO₂ films with irregularly spherical Ag NPs, the maximum enhancement factors were determined to be 1×10^6 and 6.9 for SERS and fluorescence, respectively. The enhancement of localized electromagnetic fields near the surface of Ag NPs is demonstrated to be responsible for the enhancement.

REFERENCES

1. M.R. Hoffmann, S.T. Martin, W. Choi, and D.W. Bahnemann: Environmental applications of semiconductor photocatalysis. *Chem. Rev.* **95**, 69 (1995).
2. X. Chen and S.S. Mao: Titanium dioxide nanomaterials: Synthesis, properties, modifications, and applications. *Chem. Rev.* **107**, 2891 (2007).
3. M. Es-Souni, M. Es-Souni, S. Habouti, N. Pfeiffer, A. Lahmar, M. Dietze, and C-H. Solterbeck: Brookite formation in TiO₂-Ag nanocomposites and visible light induced templated growth of Ag nanostructures in TiO₂. *Adv. Funct. Mater.* **20**, 377 (2010).
4. K. Awazu, M. Fujimaki, C. Rockstuhl, and J. Tominaga: A plasmonic photocatalyst consisting of silver nanoparticles embedded in titanium dioxide. *J. Am. Chem. Soc.* **130**, 1676 (2008).
5. W. Hou and S.B. Cronin: A review of surface plasmon resonance-enhanced photocatalysis. *Adv. Funct. Mater.* **23**, 1612 (2013).
6. Y. Tian and T. Tatsuma: Mechanisms and applications of plasmon-induced charge separation at TiO₂ films loaded with gold nanoparticles. *J. Am. Chem. Soc.* **127**, 7632 (2005).

7. Z. Liu, W. Hou, P. Pavaskar, M. Aykol, and S.B. Cronin: Plasmon resonant enhancement of photocatalytic water splitting under visible illumination. *Nano Lett.* **11**, 1111 (2011).

8. Y. Ohko, T. Tatsuma, T. Fujii, K. Naoi, C. Niwa, Y. Kubota, and A. Fujishima: Multicolour photochromism of TiO₂ films loaded with silver nanoparticles. *Nat. Mater.* **2**, 29 (2003).

9. I. Tanahashi, H. Iwagishi, and G. Chang: Localized surface plasmon resonance sensing properties of photocatalytically prepared Au/TiO₂ films. *Mater. Lett.* **62**, 2714 (2008).

10. D.W. Li, L.J. Pan, S. Li, K. Liu, S.F. Wu, and W. Peng: Controlled preparation of uniform TiO₂-catalyzed silver nanoparticle films for surface-enhanced Raman scattering. *J. Phys. Chem. C* **117**, 6861 (2013).

11. A. Mills, G. Hill, M. Stewart, D. Graham, W.E. Smith, S. Hodgen, P.J. Halfpenny, K. Faulds, and P. Robertson: Characterization of novel Ag on TiO₂ films for surface-enhanced Raman scattering. *Appl. Spectrosc.* **58**, 922 (2004).

12. I. Tanabe, K. Matsubara, S.D. Stridge, E. Kazuma, and K.L. Kelly: Photocatalytic growth and plasmon resonance-assisted photoelectrochemical toppling of upright Ag nanoplates on a nanoparticulate TiO₂ film. *Chem. Commun.* **24**, 3621 (2009).

13. K. Matsubara, K.L. Kelly, N. Sakai, and T. Tatsuma: Plasmon resonance-based photoelectrochemical tailoring of spectrum, morphology and orientation of Ag nanoparticles on TiO₂ single crystals. *J. Mater. Chem.* **19**, 5526 (2009).

14. E. Kazuma, K. Matsubara, K.L. Kelly, N. Sakai, and T. Tatsuma: Bi- and uniaxially oriented growth and plasmon resonance properties of anisotropic Ag nanoparticles on single crystalline TiO₂ surfaces. *J. Phys. Chem. C* **113**, 4758 (2009).

15. R. Viswanatha, P.K. Santra, C. Dasgupta, and D.D. Sarma: Growth mechanism of nanocrystals in solution: ZnO, a case study. *Phys. Rev. Lett.* **98**, 255501 (2007).

16. A. Moores and F. Goettmann: The plasmon band in noble metal nanoparticles: An introduction to theory and applications. *New J. Chem.* **30**, 1121 (2006).

17. T. Ung, L.M. Liz-Marza, and P. Mulvaney: Optical properties of thin films of Au@SiO₂ particles. *J. Phys. Chem. B* **105**, 3441 (2001).

18. R. Jin, Y.C. Cao, E. Hao, G.S. Me, G.C. Schatz, and C.A. Mirkin: Controlling anisotropic nanoparticles growth through plasmon excitation. *Science* **425**, 487 (2004).

19. Y. Sakai, I. Tanabe, and T. Tatsuma: Orientation-selective removal of upright Ag nanoplates from a TiO₂ film. *Nanoscale* **3**, 4101 (2011).

20. I. Tanabe, K. Matsubara, N. Sakai, and T. Tatsuma: Photoelectrochemical and optical behavior of single upright Ag nanoplates on a TiO₂ film. *J. Phys. Chem. C* **115**, 1695 (2011).

21. S. Li, Q. Tao, D.W. Li, and Q.Y. Zhang: Controlled anisotropic growth of Ag nanoparticles on oil-decorated TiO2 films with photocatalytic reduction method. *J. Mater. Res.* **29**, 2497 (2014).

22. M. Ohring: *Materials Science of Thin Films: Deposition and Structure* (Academic Press, San Diego, 2002).

23. S. Yin, F. Huang, J. Zhang, J. Zheng, and Z. Lin: The effects of particle concentration and surface charge on the oriented attachment growth kinetics of CdTe nanocrystals in H₂O. *J. Phys. Chem. C* **115**, 10357 (2011).

24. K.L. Kelly, E. Coronado, L.L. Zhao, and G.C. Schatz: The optical properties of metal nanoparticles: The influence of size, shape, and dielectric environment. *J. Phys. Chem. B* **107**, 668 (2003).

25. E. Prodan, C. Radloff, N.J. Halas, and P. Nordlander: A hybridization model for the plasmon response of complex nanostructures. *Science* **302**, 419 (2003).

26. F.J. Beck, E. Verhagen, S. Mokkapati, A. Polman, and K.R. Catchpole: Resonant SPP modes supported by discrete metal nanoparticles on high-index substrates. *Opt. Express* **19**(S2), A146 (2011).

27. P. Hildebrandt and M. Stockburger: Surface-enhanced resonance Raman-spectroscopy of rhodamine-6G adsorbed on colloidal silver. *J. Phys. Chem.* **88**, 5935 (1984).

28. Q. Tao, S. Li, Q.Y. Zhang, D.W. Kang, J.S. Yang, W.W. Qiu, and K. Liu: Controlled growth of ZnO nanorods on textured silicon wafer and the application for highly effective and recyclable SERS substrate by decorating Ag nanoparticles. *Mater. Res. Bull.* **54**, 6 (2014).

29. F.J. Garcia-Vidal and J.B. Pendry: Collective theory for surface enhanced Raman scattering. *Phys. Rev. Lett.* **77**, 1163–1166 (1996).

30. Y. Yang, S. Matsubara, L.M. Xiong, T. Hayakawa, and M. Nogami: Solvothermal synthesis of multiple shapes of silver nanoparticles and their SERS properties. *J. Phys. Chem. C* **111**, 9095–9104 (2007).

31. J.R. Lakowicz, C.D. Geddes, I. Gryczynski, J. Malicka, Z. Gryczynski, K. Aslan, J. Lukomska, E. Matveeva, J. Zhang, R. Badugu, and J.J. Huang: Advances in surface-enhanced fluorescence. *J. Fluoresc.* **14**, 425 (2004).

32. J.R. Lakowicz: Radiative decay engineering 5: Metal-enhanced fluorescence and plasmon emission. *Anal. Biochem.* **337**, 171 (2005).

Supplementary Material

To view supplementary material for this article, please visit http://dx.doi.org/10.1557/jmr.2014.378.